



Research paper

Generalized intergranular strain concept and its application to hypoplastic models

L. Mugele^{a,*}, H.H. Stutz^a, D. Mašín^b^a Institute of Soil Mechanics and Rock Mechanics (IBF), Karlsruhe Institute of Technology (KIT), Karlsruhe, Germany^b Faculty of Science, Charles University, Prague, Czech Republic

ARTICLE INFO

Dataset link: www.soilmodels.com

Keywords:

Hypoplasticity
 Intergranular strain
 Generalized intergranular strain
 Small-strain stiffness
 Asymptotic state boundary surface

ABSTRACT

This work presents a generalized approach for the consideration of small-strain effects in constitutive models for soils. These are thereby particularly important for the simulation of cyclic deformations of soil subjected to small strain amplitudes. The novel generalized intergranular strain (GIS) approach represents an overlay concept for constitutive models and is based on the well-known intergranular strain (IS) concept after Niemunis and Herle (1997), resp. its improvement (ISI) after Duque et al. (2020). However, the novel GIS concept can easily be transferred to different constitutive models (e.g. hypoplastic or elasto-plastic formulations). Based on an extended generalized hypoplastic formulation, the GIS concept is combined with the base hypoplastic constitutive model for sand after von Wolffersdorff (1996) (HP) incorporating the extracted asymptotic state boundary surface (ASBS). The latter is derived and visualized. Different element test simulations with the coupled HP+GIS model and the well-known HP+IS formulation are presented and compared using a parameter set of Zbraslav sand. Thereby, the intrinsic feature of the GIS concept, which prevents overshooting of the ASBS, becomes apparent. Based on the ISI formulation, nonlinear accumulation effects can be reproduced in the GIS concept using a further scalar historirotopic state variable.

1. Introduction

The constitutive modeling of granular media, such as sand, still remains a significant challenge in theoretical and computational soil mechanics. Consequently, numerous constitutive models have been developed over the last decades. It is worth mentioning that different families of constitutive models have emerged with the most relevant being elasto-plastic and hypoplastic formulations. A particular challenge in modeling the stress–strain behavior of soil involves so-called *small-strain effects*. These become especially relevant if the soil is subjected to cyclic deformations (Benz et al., 2009a; Cudny and Truty, 2020). Small-strain effects in combination with hypoplastic constitutive formulation are the main focus of this work.

Hypoplastic constitutive models are generally characterized by the absence of a fully elastic region. Irreversible (plastic) deformations and also contractancy and dilatancy effects can thus be simulated. In hypoplastic formulations, irreversible deformations occur due to the mathematical consideration of the norm of the strain rate $\|\dot{\epsilon}\|$ instead of the plastic strain rate $\dot{\epsilon}^{\text{pl}}$ in elasto-plastic models. A decomposition of the strain rate into an elastic and a plastic part, as known from elasto-plasticity, does not exist in hypoplastic models. Hence, no yield surface, no plastic potential (for the calculation of the elasto-plastic

flow rule), and no plastic multiplier need to be defined. Hypoplastic constitutive models can be expressed using a single tensorial equation, which interrelates the rate of the effective Cauchy stress $\dot{\sigma}$ (objective Zaremba-Jaumann stress rate $\dot{\sigma}$ to be precise) with the strain rate $\dot{\epsilon}$ (Euler stretching tensor \mathbf{D} in general). Additionally, hypoplastic constitutive models are characterized by a straightforward numerical implementation and a realistic bifurcation (shear band prediction). These characteristics render hypoplastic models fundamentally suitable for simulating the mechanical behavior of soil.

Early hypoplastic formulations considered only the effective stress σ as state variable (Kolymbas, 1988, 1991a,b; Wu and Bauer, 1994). By introducing the void ratio e as an additional state variable, hypoplastic formulations have been developed that can represent the non-linear soil behavior, *contractancy*, and *dilatancy* as well as density and pressure dependency (*Pyknotropy* and *Barotropy*) (Bauer, 1996; Gudehus, 1996; Wu et al., 1996). The version of hypoplasticity according to von Wolffersdorff (1996) (HP) implemented the limit condition by Matsuoka and Nakai (1977) and is probably the most widely used hypoplastic model for granular materials with the two state variables mentioned above. The complexity of the mechanical behavior of soil further increases when considering load direction reversals or cyclic loading. It revealed

* Corresponding author.

E-mail addresses: luis.mugele@kit.edu (L. Mugele), hans.stutz@kit.edu (H.H. Stutz), masin@natur.cuni.cz (D. Mašín).

that the aforementioned state variables are not sufficient for describing cyclic deformations in hypoplastic models. Therefore, the tensorial state variable *intergranular strain* h was introduced using the intergranular strain concept (IS) by Niemunis and Herle (1997) for the consideration of the recent strain history. In this way, the so-called *ratcheting* could be prevented for certain stress or strain amplitudes by the coupled hypoplastic formulation HP+IS. Nowadays, HP+IS is still widely used to simulate problems with numerous loading cycles and decisive accumulative effects (Osinov, 2005; Chrisopoulos and Vogelsang, 2019; Norlyk et al., 2020; Machaček et al., 2021; Staubach et al., 2021), although a number of enhancements have been developed since then (see Section 4). For example, an additional scalar state variable was introduced by Poblete et al. (2016) and Duque et al. (2020) for modeling the so-called *historiotropic* effects. Historiotropic effects involve the response of the soil depending on the (cyclic) preloading history. For example, they can be seen in the *s-shaped curves* of pore fluid pressure accumulation in cyclic undrained triaxial tests (Duque et al., 2023a,b).

However, it should be mentioned that both parts of the HP+IS reveal several shortcomings. The ones related to the base constitutive model HP include (I) the insufficient reproduction of dilatancy effects, (II) the possible accessibility of tensile stress states in dense states, (III) the incorporation of a hypoelastic stiffness instead of a hyperelastic one, and (IV) the lack of a further state variable for considering the current structure (so-called *fabric*) of the soil. These issues have been discussed and addressed in neohypoplasticity (NHP) (Niemunis et al., 2016; Niemunis and Grandas-Tavera, 2019; Mugele et al., 2024b,a). The shortcomings of overlay model IS include (I) the so-called *overshooting* due to a single un- and reloading cycle, (II) the possible accessibility of tensile stress states due to multiple loading and unloading cycles, (III) an inadequate modeling of accumulation effects, and (IV) a non-trivial extension of the concept to other hypoplastic as well as non-hypoplastic formulations (Osinov, 2017; Bode et al., 2020; Duque et al., 2022; Tafili et al., 2024). Some of the deficits mentioned in both HP and IS can lead to serious misinterpretations of numerical simulations.

Considering the base constitutive model first, an extended generalized hypoplastic formulation is proposed in Section 2. The proposed equation can be applied to hypoplastic models with an explicitly defined, extracted as well as a non-existent so-called *asymptotic state boundary surface* (ASBS). The ASBS summarizes all states in the stress-void ratio space, which will be reached upon a sufficient long monotonic stretching (Mašín and Herle, 2005; Mašín, 2009). Based on the development of rate-independent hypoplastic formulations for clay (Mašín, 2005; Mašín and Herle, 2005), Mašín introduced hypoplastic constitutive formulations for fine-grained soils including an explicitly defined ASBS (Mašín and Herle, 2006; Mašín, 2012, 2013). Although such ASBS exists in sand (Mašín and Herle, 2006), no hypoplastic sand model has been developed incorporating a defined or even an extracted ASBS. Therefore, in Section 3, the HP model is reformulated using the extracted ASBS.

For the simulation of cyclic loading, an extension of the base constitutive model is needed. After providing an overview of the original IS concept in Section 4, the proposed so-called *generalized intergranular strain* (GIS) is introduced in Section 5. Finally, in Section 6, the performance of the GIS concept is analyzed using numerical element tests. The coupled model HP+GIS is used as an example and its corresponding simulations are compared against the original version of HP+IS. The notation and abbreviations used in this paper are summarized in Appendix A.

2. Extended generalized hypoplasticity

The theory of hypoplasticity is based on a general representation theorem of isotropic tensorial functions of two symmetric tensorial arguments $(\sigma, \dot{\epsilon})$ in combination with some general mathematical restrictions (homogeneity of one in $\dot{\epsilon}$). The first suitable rate-independent hypoplastic constitutive models for soil incorporated only the effective

Cauchy stress σ as state variable were found by heuristic guessing, i.e. systematic trial and error by Kolymbas (1988, 1991a,b). Based on this, the tensorial equation between the stress rate $\dot{\sigma}$ of the effective Cauchy stress σ and the strain rate $\dot{\epsilon}$ for a hypoplastic formulation was established historically by Wu (1992) and Wu and Bauer (1994):

$$\dot{\sigma} = L : \dot{\epsilon} + N \|\dot{\epsilon}\|. \quad (1)$$

Thereby, the fourth order tensor L , which is known as a *linear term*, and the second order tensor N , which is known as a *non-linear term*, are both functions of the effective Cauchy stress. Using the barotropy factor f_s as well as the pyknotropy factor f_d and introducing the void ratio e as an additional state variable, the influence of density and pressure on the mechanical behavior of soil could be taken into account by Bauer (1996) and Gudehus (1996). The resulting mathematical form

$$\dot{\sigma} = f_s L : \dot{\epsilon} + f_s f_d N \|\dot{\epsilon}\| \quad (2)$$

often serves as the basis for the formulation of hypoplastic constitutive models until today. Only rate-independent hypoplastic formulations such as von Wolffersdorff (1996), Mašín (2005), Grandas-Tavera et al. (2020), Liao and Yang (2021), Liao et al. (2022), Mugele et al. (2024b) are considered in the present paper, which are characterized by the degree of homogeneity of one with respect to the strain rate (Gudehus, 2007; Mašín, 2019). Although rate-dependent so-called *visco-hypoplastic* models have also been developed (Niemunis et al., 2009; Jerman and Mašín, 2020).

Let us now focus on a specific property of the mechanical behavior of the soil. A so-called *asymptotic state* is a state of the soil, which is reached upon a sufficiently long monotonic deformation (Gudehus, 2007; Mašín, 2019). When plotted in stress-void ratio space, asymptotic states (also known as *swept-out-memory* (SOM) states or *attractors* (Gudehus, 2007; Gudehus and Mašín, 2009)) lie on the asymptotic state boundary surface (ASBS). So-called *Critical states* reveal one specific asymptotic state which is reached asymptotically upon a proportional volume preserving strain path.

For simplicity, only models, in which the state of the soil is described as unique using the effective Cauchy stress σ and the void ratio e , are considered in the following. In general, the ASBS for such models represents a geometric object and the current state a point in the general 4D stress-void ratio space (4-dimensional vector space \mathbb{R}^4). Although this 4D space is difficult to imagine, it must exist as an extension of the 3D stress space (\mathbb{R}^3). Note that for example the 4D principal stress-void ratio $(\sigma_1 \sigma_2 \sigma_3 e)$ space or the 4D mean effective pressure - deviatoric stress - Lode angle - void ratio $(pq\theta e)$ space using the Roscoe-Invariants p, q and the Lode angle θ can thereby be used. The well-known 2D spaces \mathbb{R}^2 , such as the pq or the ep diagram, can be derived directly from the aforementioned generalized 4D space. In elasto-plastic models, this ASBS coincides with the state boundary surface, which is formed by combining the yield surface and a hardening law (Mašín, 2012).

Generally, hypoplastic constitutive models can also be written incorporating an explicitly defined ASBS (Mašín, 2012). Fig. 1 shows as an example the ASBS for the rate-independent hypoplastic formulations for clay by Mašín (2013) with explicitly defined asymptotic states in the principal 3D stress space. In Mašín (2013), the shape of the ASBS is defined as invariant for constant void ratio cross sections. It should be noted that the shape of cross sections with constant mean effective pressure, constant Lode angle or constant deviatoric stress is not invariant due to the considered Matsuoka-Nakai criterion (Matsuoka and Nakai, 1977). Irreversible densification is thereby scaling the size but not changing the shape of the ASBS (Mašín, 2019). The assumed invariant shape with respect to the void ratio of the ASBS seems to be reasonable for clay but not for sand.

As demonstrated by Mašín (2012), the general form of a hypoplastic model formulated using an explicitly defined ASBS is

$$\dot{\sigma} = f_s L : \dot{\epsilon} - \frac{f_d}{f_d^A} A : \mathbf{d} \|\dot{\epsilon}\|. \quad (3)$$

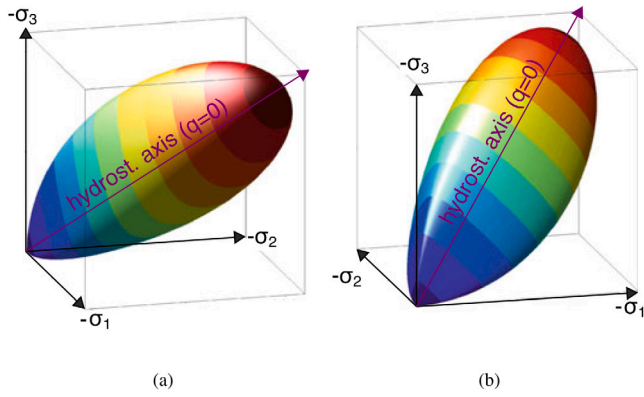


Fig. 1. 3D plots in the principal stress space of the ASBS for the hypoplastic formulation for clay (Mašín, 2013) for (a) and (b) views from various angles with constant mean stress cuts displayed using different colors, modified from Mašín (2013).

Thereby the fourth-order tensor L denotes the linear stiffness (a hypoplastic stiffness is often used for simplicity) and the fourth-order tensor A can be calculated using the defined asymptotic states. The tensor A incorporates the stiffness upon loading for states at the ASBS. It controls the inclination of an arbitrary normal compression line (NCL) in the ep plane and therefore changes the size and possibly also the shape of the ASBS. f_d^A denotes the value of the pyknropy factor f_d for a given state at the ASBS (the superscript \sqcup^A denotes a state on the ASBS). The Quotient f_d / f_d^A can be interpreted as the normalized distance of the current state from the ASBS. The behavior of the material becomes more 'elastic' for states inside and with greater distance from the ASBS. On each point on the ASBS $f_d / f_d^A = 1$ applies. The second order tensor d can be calculated using the asymptotic strain rate $\dot{\epsilon}^A$ corresponding to the given state projected on the ASBS:

$$d = \frac{\dot{\epsilon}^A}{\|\dot{\epsilon}^A\|} = \bar{\epsilon}^A. \quad (4)$$

The described mathematical formulation and the corresponding projection of a given state on the ASBS of hypoplastic models with explicitly defined ASBS is illustrated in simplified form in Fig. 2 for the triaxial case (pq diagram).

If an ASBS is explicitly defined, such as in the models for clay (Mašín, 2012, 2013), the fourth order tensor A is specified and the pyknropy factor f_d^A can be calculated directly. However, using

$$N = -\frac{A : d}{f_s f_d^A}, \quad (5)$$

Eq. (3) can be rewritten using the well-known second-order tensor N :

$$\dot{\sigma} = f_s L : \dot{\epsilon} + f_s \frac{f_d}{f_d^A} f_d^A N \|\dot{\epsilon}\|. \quad (6)$$

Unlike Eq. (3), Eq. (6) can be used also for any hypoplastic model in the form of Eq. (2) for which the pyknropy factor in the asymptotic state f_d^A can be extracted but which has not been defined using Eq. (3) explicitly. This allows, for example, to express the widely used hypoplastic model for sand after von Wolffersdorff (HP) in the form of Eq. (6), see Section 3.

Based on the *generalized hypoplasticity* proposed by Niemunis (2003), a further *extended generalized hypoplasticity* can be proposed

$$\dot{\sigma} = E : (\dot{\epsilon} - m C S \|\dot{\epsilon}\| + f(\dot{\epsilon}, \alpha)). \quad (7)$$

In Eq. (7), E represents the elastic (hypo-, or hyper-elastic, the latter being preferred) stiffness, m is the hypoplastic flow rule, and S a variable called *state mobilization*. The state mobilization S represents a ratio between the current state and a defined reference state. Note that for clay models the quantity $1/S$ can be interpreted as the well-known *overconsolidation ratio* (Bode et al., 2021; Niemunis, 2003). A

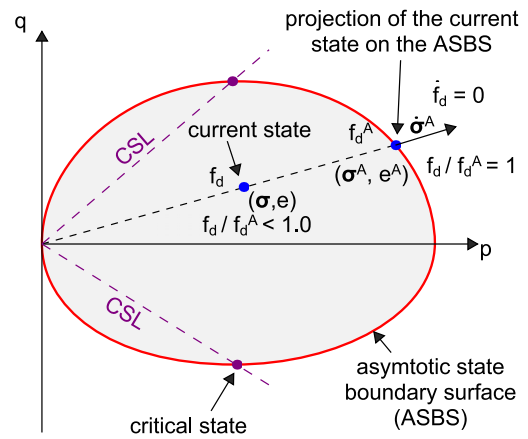


Fig. 2. Simplified schematic representation of the projection of a current state on the corresponding state on the ASBS of hypoplastic constitutive formulations with explicitly defined ASBS in the triaxial case (pq diagram), modified from Mašín (2019).

constitutive model according to Eq. (6) can be reformulated into Eq. (7) using

$$E = L f_s, \quad (8)$$

$$m = -[L^{-1} : N], \quad (9)$$

$$C = \|L^{-1} : N\| f_d^{A*}, \quad (10)$$

$$S = f_d / f_d^{A*}, \quad (11)$$

$$f(\dot{\epsilon}, \alpha) = 0. \quad (12)$$

If f_d^A can be calculated explicitly, one gets $f_d^{A*} = f_d^A$. If f_d^A cannot be calculated explicitly for a given state, in several models a likewise quantity f_d^{A*} can be defined, see Section 3. For models in which neither f_d^A nor f_d^{A*} can be derived however Eq. (2) holds, $S = Y$ can be specified. In this case, Y is known as the so-called *degree of non-linearity* (Niemunis, 2003). This applies, for instance, to models which only consider the effective stress as a state variable. For such models,

$$C = 1, \quad (13)$$

$$S = Y = f_d \|L^{-1} : N\| \quad (14)$$

can be used instead of Eq. (10) and Eq. (11). Obviously, models in which f_d^{A*} can be determined can also be expressed using the degree of nonlinearity Y (Niemunis, 2003). However, as will be discussed later, using $S = f_d / f_d^{A*}$ is preferred, as $S = 1.0$ applies for every state on the ASBS. In contrast, $Y = 1.0$ only holds at the failure state defined by $\dot{\sigma} = 0$, and asymptotically only in the critical state, one specific asymptotic state due to a volume-constant proportional strain path.

The function $f(\dot{\epsilon}, \alpha)$ and the scalar parameter C are introduced for the purpose of generalization, although $f(\dot{\epsilon}, \alpha) = 0$ holds for most constitutive formulations mentioned until now. Note that $f(\dot{\epsilon}, \alpha) \neq 0$ applies in the recently published neohypoplasticity (NHP) (Niemunis et al., 2016; Niemunis and Grandas-Tavera, 2019; Mugele et al., 2024b). Similarly, $f(\dot{\epsilon}, \alpha)$ can generally depend on all state variables α and needs to be homogeneous of the first order concerning the strain rate to ensure rate-independent material behavior. Note that α includes at least the effective Cauchy stress σ and the void ratio e in most advanced constitutive models for soil. In addition, $f(\dot{\epsilon}, \alpha) = 0$ is requested in asymptotic states.

3. Reformulation of HP using the extracted ASBS

Hypoplastic constitutive models for clay have already been formulated using an explicitly defined ASBS (Mašín, 2012, 2013; Mašín and Rott, 2014; Mašín, 2014, 2019). However, when considering the HP for sand, it becomes apparent that although an ASBS exists in the model, its explicit definition and thus the reformulation of the HP into the form of Eq. (3) is nontrivial (Mašín and Herle, 2006). Therefore, the ASBS is extracted from the HP first. All corresponding mathematical equations of HP can be found in Appendix B. Using the extracted ASBS, the HP formulation can finally be expressed using Eq. (6).

Below, the superscript \sqcup^A denotes a state on the ASBS. The HP model involves two state variables: the effective Cauchy stress σ and the void ratio e . It is assumed in the following that a given state lies on the ASBS and therefore $\sigma^A = \sigma$ and $e^A = e$ applies. It is further assumed, that the stress rate $\dot{\sigma}^A$ has the same direction as the stress tensor σ^A . It follows, that the pyknotropy factor must be constant ($\dot{f}_d^A = 0$) for a particular direction of the strain rate $\dot{\bar{\epsilon}}^A$. This requirement corresponds to the well-known *normal compression line* (NCL) in the ep space. For a given state, the asymptotic pyknotropy factor f_d^A is derived using the approach after Mašín and Herle (2006). On the ASBS $\dot{\sigma}^A \parallel \sigma^A$ holds and a scalar multiplier γ can be introduced

$$\dot{\sigma}^A = \gamma \bar{\sigma}^A. \quad (15)$$

Furthermore, $\dot{f}_d = 0$ holds. $\|\dot{\bar{\epsilon}}^A\| = 1$ can be assumed in the asymptotic state for rate-independent constitutive formulations. Consequently, a hypoplastic constitutive formulation of the form of Eq. (2) can be written in the asymptotic state:

$$\gamma \bar{\sigma}^A = f_s^A \mathbf{L} : \bar{\bar{\epsilon}}^A + f_s^A f_d^A \mathbf{N}. \quad (16)$$

It is worth to mention that this general equation applies for $\dot{\bar{\epsilon}}_{\text{vol}}^A > 0$ ($\gamma < 0$) as well as for $\dot{\bar{\epsilon}}_{\text{vol}}^A < 0$ ($\gamma > 0$). In the critical state, $\dot{\sigma}^A = 0$, hence $\gamma = 0$ holds. The pyknotropy factor f_d is defined as

$$f_d = \left(\frac{e - e_d}{e_c - e_d} \right)^\alpha \quad (17)$$

with the characteristic pressure-dependent void ratios in the critical state e_c and in the densest state e_d . These evolve within the HP formulation with the mean effective pressure according to Bauer's compression law (Bauer, 1996):

$$\frac{e_c}{e_{c0}} = \frac{e_d}{e_{d0}} = \exp \left[- \left(\frac{3p}{h_s} \right)^n \right]. \quad (18)$$

The void ratios e_{c0} and e_{d0} represent thereby the corresponding void ratios at zero mean effective pressure whereby the exponent n and the granular hardness h_s are constitutive parameters. On the ASBS, the pyknotropy factor f_d^A for any NCL, which is defined by

$$e^A = e_0^A \exp \left[- \left(\frac{3p^A}{h_s} \right)^n \right], \quad (19)$$

is constant. Differentiation with respect to time leads to

$$\frac{\dot{e}^A}{e^A} = \frac{n}{h_s} \text{tr}(\dot{\sigma}^A) \left(\frac{3p^A}{h_s} \right)^{(n-1)}. \quad (20)$$

The volumetric strain rate in the asymptotic state

$$\dot{\bar{\epsilon}}_{\text{vol}}^A = \text{tr} \left(\bar{\bar{\epsilon}}^A \right) \quad (21)$$

can be expressed by using the evolution of the void ratio

$$\dot{e}^A = (1 + e^A) \text{tr} \left(\bar{\bar{\epsilon}}^A \right). \quad (22)$$

Combining Eq. (15), Eq. (20), and Eq. (22) leads to

$$\text{tr}(\bar{\bar{\epsilon}}^A) \left(\frac{1 + e^A}{e^A} \right) = \gamma \frac{n}{h_s} \text{tr} \bar{\sigma}^A \left(\frac{3p^A}{h_s} \right)^{(n-1)}. \quad (23)$$

The system of Eqs. (16) and (23) can further be used to determine f_d^A . For this purpose, $\bar{\bar{\epsilon}}^A$ can be eliminated. Eq. (16) can be rewritten to:

$$\bar{\bar{\epsilon}}^A = \gamma / f_s^A \left(\mathbf{L}^{-1} : \bar{\sigma}^A \right) - f_d^A \left(\mathbf{L}^{-1} : \mathbf{N} \right). \quad (24)$$

Combining Eq. (23) with Eq. (24) yields

$$\gamma = - \frac{\left(\frac{1+e^A}{e^A} \right) \text{tr} \mathbf{B}}{G - \left(\frac{1+e^A}{e^A} \right) \text{tr} \mathbf{C}} f_d^A \quad (25)$$

using

$$\mathbf{B} = \mathbf{L}^{-1} : \mathbf{N}, \quad (26)$$

$$\mathbf{C} = 1 / f_s^A (\mathbf{L}^{-1} : \bar{\sigma}^A), \quad (27)$$

$$G = \frac{n}{h_s} \text{tr} \bar{\sigma}^A \left(\frac{3p^A}{h_s} \right)^{(n-1)}. \quad (28)$$

$\|\bar{\bar{\epsilon}}^A\| = 1$ can be applied to Eq. (24). It leads to

$$1 = \sqrt{(\gamma \mathbf{C} - f_d^A \mathbf{B})^2} \quad (29)$$

or

$$1 = \|\mathbf{B}\|^2 (f_d^A)^2 + \|\mathbf{C}\|^2 \gamma^2 - 2(\mathbf{B} : \mathbf{C}) f_d^A \gamma. \quad (30)$$

Finally, the scalar multiplier γ can be eliminated by substituting Eq. (25) into Eq. (30). The resulting pyknotropy factor in the asymptotic state f_d^A for the HP formulation reads (Mašín and Herle, 2006):

$$f_d^A = \sqrt{\left[\|\mathbf{B}\|^2 + \frac{\left(\frac{\|\mathbf{C}\| \left(\frac{1+e^A}{e^A} \right) \text{tr} \mathbf{B}}{G - \left(\frac{1+e^A}{e^A} \right) \text{tr} \mathbf{C}} \right)^2}{G - \left(\frac{1+e^A}{e^A} \right) \text{tr} \mathbf{C}} + \frac{2(\mathbf{B} : \mathbf{C}) \text{tr} \mathbf{B} \left(\frac{1+e^A}{e^A} \right)}{G - \left(\frac{1+e^A}{e^A} \right) \text{tr} \mathbf{C}} \right]^{-1}}. \quad (31)$$

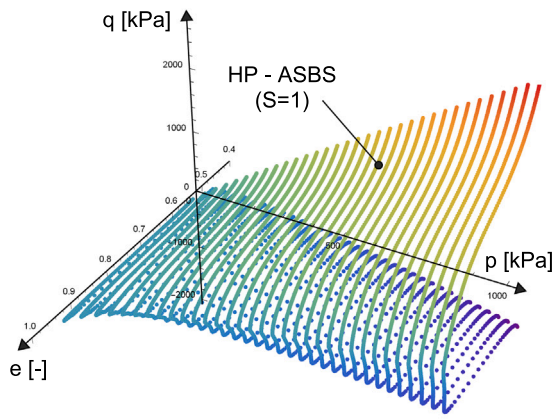
For the corresponding relative void ratio in the asymptotic state r_e^A applies:

$$r_e^A = \left(\frac{e^A - e_d}{e_c - e_d} \right) = (f_d^A)^{(1/\alpha)} \quad (32)$$

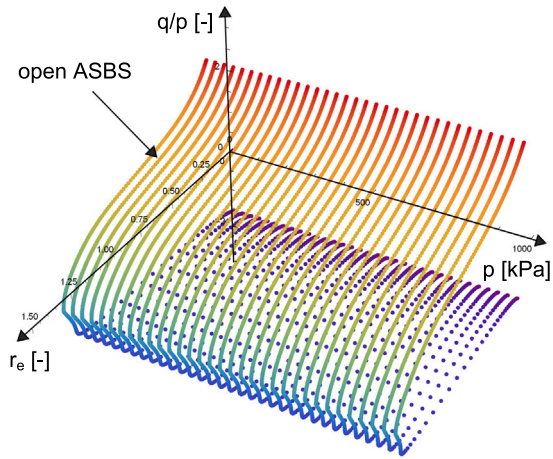
It is evident that f_d^A resp. r_e^A according to Eq. (31) resp. Eq. (32) depends on both the effective stress and the void ratio. It should also be noted that the barotropy factor in the asymptotic state f_s^A also influences f_d^A , see Eq. (27). Thus, for a given state, the pyknotropy factor in the asymptotic state f_d^A in the HP cannot be calculated explicitly. Eq. (31) is an implicit expression for f_d^A . However, it is shown in the following that the ASBS of the HP formulation can be found numerically and f_d^{A*} can be defined as described in Section 2.

Assuming that a current state (σ, e) is located on the ASBS, a value of the pyknotropy factor in a projected asymptotic state f_d^{A*} can be calculated by setting $\sigma^A = \sigma$ and $e^A = e$ in Eq. (31). For an asymptotic state, $f_d^{A*} = f_d^A$ applies. The comparison of f_d^{A*} with the current value of the pyknotropy factor f_d (Eq. (17)) enables the determination of the state mobilization S . If $S = f_d / f_d^{A*} = 1 = f_d / f_d^A$ applies for a current state, the latter is located on the ASBS. However, such states on the ASBS can in general only be found numerically as described above.

The resulting ASBS in the HP model for sand is studied for the triaxial stress state in different vector spaces. The used constitutive parameters of Zbraslav sand can be found in Table 1. Fig. 3a shows the resulting ASBS in 3D (\mathbb{R}^3) epq space while Fig. 3b presents the ASBS in the corresponding normalized $r_e pq/p$ space. Fig. 4 illustrates corresponding 2D cross sections (\mathbb{R}^2) for a constant void ratio (Fig. 4a) and a constant mean effective pressure (Fig. 4b). The described non-invariant shape of the ASBS is obvious. The shape of the ASBS varies both for constant void ratio cross sections and (slightly) for constant mean effective pressure cross sections. Furthermore, a special charac-



(a)



(b)

Fig. 3. ASBS for the HP model for sand in the (a) 3D epq space and the (b) normalized 3D $r_e pq/p$ space for triaxial conditions.

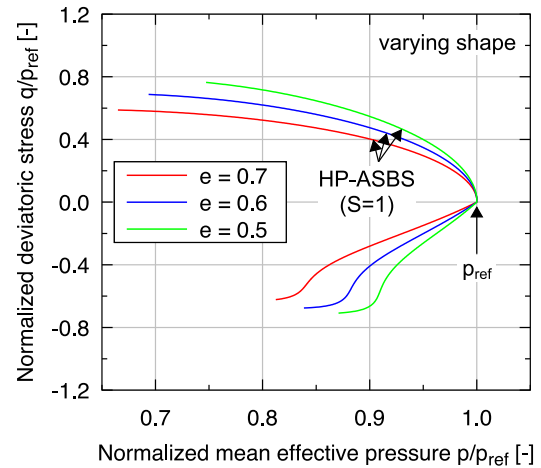
teristic of sand should be emphasized: the ASBS is open for $p \rightarrow 0$, see Fig. 3b.

According to Eq. (6), the HP can be reformulated incorporating the extracted ASBS. To demonstrate the feasibility of the model, the state mobilization $S = f_d/f_d^{A*}$ is calculated for a variable triaxial stress state (p, q) with a chosen constant void ratio of $e = 0.6$. The resulting distribution of $S = f_d/f_d^{A*} = f(p, q)$ can be seen in Fig. 5. Only states for $S \leq 1.0$ are plotted, allowing the ASBS ($S = 1$) to be seen. The edge with $S = 1$ represents the ASBS in the well-known pq diagram. It is evident that the latter has an realistic shape for the considered case and $S < 1.0$ holds for all states within the ASBS.

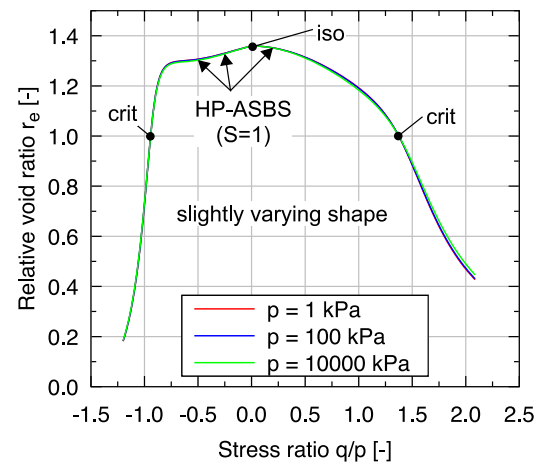
4. Intergranular strain concept (IS)

The hypoplastic models which have been discussed in detail so far can be used to simulate monotonic deformations. However, an overlay model is required to simulate cyclic deformations. In the following the intergranular strain (IS) concept after Niemunis and Herle (1997) is briefly introduced. The tensorial and strain-like state variable of the so-called intergranular strain \mathbf{h} memorizes the current strain history. The evolution of \mathbf{h} can be expressed as

$$\dot{\mathbf{h}} = \begin{cases} (\mathbf{I} - \tilde{\mathbf{h}}\tilde{\mathbf{h}}\rho^{\beta_r}) : \dot{\boldsymbol{\varepsilon}} & \text{if } \tilde{\mathbf{h}} : \dot{\boldsymbol{\varepsilon}} > 0 \\ \dot{\boldsymbol{\varepsilon}} & \text{if } \tilde{\mathbf{h}} : \dot{\boldsymbol{\varepsilon}} \leq 0 \end{cases} \quad (33)$$

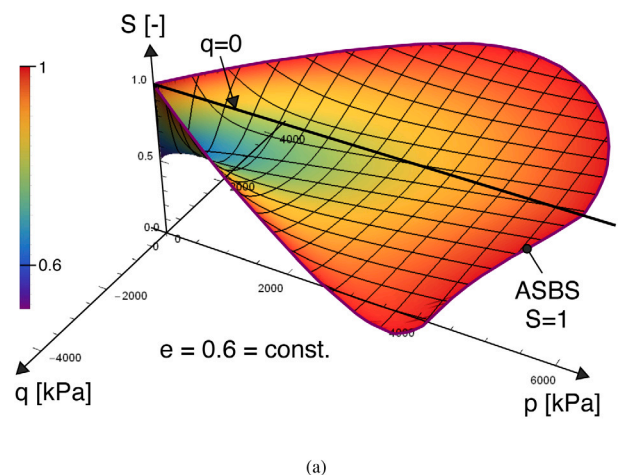


(a)



(b)

Fig. 4. Normalized ASBS for HP model for sand for triaxial conditions in 2D (a) constant void ratio cross sections and (b) constant mean effective pressure cross sections.



(a)

Fig. 5. State mobilization $S = f_d/f_d^{A*}$ for a constant void ratio $e = 0.6$ in a triaxial stress state (p, q) in the reformulated HP model for sand with extracted ASBS.

whereby the parameter β_R controls the evolution of \mathbf{h} . The direction of intergranular strain $\vec{\mathbf{h}}$ is formulated as

$$\vec{\mathbf{h}} = \begin{cases} \frac{\mathbf{h}}{\|\mathbf{h}\|} & \text{if } \mathbf{h} \neq 0 \\ 0 & \text{if } \mathbf{h} = 0 \end{cases} \quad (34)$$

and the normalized degree of mobilization of the intergranular strain $0 \leq \rho \leq 1$ can be calculated using

$$\rho = \frac{\|\mathbf{h}\|}{R}, \quad (35)$$

whereby the parameter R quantifies the elastic range. For monotonic deformations, the direction of \mathbf{h} tends to $\dot{\epsilon}$ and its norm asymptotically reaches R .

The original concept of intergranular strain was developed as an overlay model for the hypoplasticity after von Wolffersdorff (1996) (HP). All corresponding mathematical equations of HP can be found in Appendix B. HP can be written as

$$\dot{\sigma} = f_s (L : \dot{\epsilon} + f_d N \|\dot{\epsilon}\|) \quad (36)$$

(Bauer, 1996; Gudehus, 1996). Using the IS concept with HP, the resulting coupled constitutive model HP+IS can be formulated as

$$\dot{\sigma} = M : \dot{\epsilon}, \quad (37)$$

whereby the tangential stiffness M of the model is interpolated using the above mentioned fourth-order tensor L and second-order tensor N as:

$$M = [\rho^\chi m_T + (1 - \rho^\chi) m_R] L + \begin{cases} \rho^\chi (1 - m_T) L : \vec{\mathbf{h}} \vec{\mathbf{h}} + \rho^\chi N \vec{\mathbf{h}} & \text{if } \vec{\mathbf{h}} : \dot{\epsilon} > 0 \\ \rho^\chi (m_R - m_T) L : \vec{\mathbf{h}} \vec{\mathbf{h}} & \text{if } \vec{\mathbf{h}} : \dot{\epsilon} \leq 0 \end{cases} \quad (38)$$

Note that in Eq. (38) the factors f_s and f_d are already included in L and N . The parameters m_R and m_T specify the stiffness increase as a function of the strain rate direction in relation to the direction and mobilization of the intergranular strain \mathbf{h} . The material parameter χ influences the interpolation in between. Due to a monotonic shearing, Eq. (37) with (38) asymptotically tends to Eq. (36). In total, there are 13 parameters for HP+IS, 8 for HP and 5 for IS.

It becomes evident from Eq. (38) that the IS extension modifies the base constitutive formulation (HP) concerning two aspects:

- Increase of the linear stiffness L , and
- Decrease of the non-linear term N , i.e. of the irreversible deformations.

This aspects results in a stiffer and more elastic constitutive response after a reversal of loading direction, which reduces the ratcheting and allows the application of HP+IS for simulating cyclic deformations (Osinov, 2005; Stutz et al., 2020; Machaček et al., 2021; Staubach et al., 2021; Wotzlaw et al., 2023).

However, the IS extension exhibits several shortcomings and therefore the described original IS concept has already been modified by several authors. In the following, the most important modifications are summarized.

Wegener and Herle (2014) enhanced the term $\rho^\chi N \vec{\mathbf{h}}$ (refer to Eq. (38)) by replacing the exponent χ with a novel parameter γ ($\gamma > \chi$). This modification leads to a reduction of the strain accumulation. However, the fixed value of γ prevents the adaptation during cycles with different strain amplitudes, which limits the model's ability to predict historirotropic effects.

Fuentes and Triantafyllidis (2015) introduced the so-called *intergranular strain anisotropy* (ISA) model, which fundamentally reformulated the original IS theory. This approach utilizes an elasto-plastic evolution of the state variable of intergranular strain and incorporates a yield surface that can be controlled using the elastic strain amplitude.

An extension to the ISA model by Poblete et al. (2016) modifies the exponent controlling the irreversible deformation due to a

change in loading direction into a function that gradually increases during repetitive cycles with small strain amplitudes and decreases during monotonic loading or cyclic loading with larger strain amplitudes. Therefore a novel state variable ϵ_a was introduced. Using this, historirotropic effects such as the well-known s-shaped pore fluid pressure accumulation curves in undrained triaxial tests with stress cycles (Duque et al., 2023a,b) can be modeled.

The approach by Poblete et al. (2016) was applied by Duque et al. (2020) to the original concept of IS proposing the so-called *intergranular strain improvement* (ISI) model. The historirotropic state variable has been renamed to Ω . In accordance with the previously described procedure, this state variable is used to modify the exponent γ . As a result, the accumulation rate changes depending on Ω and the historirotropic effects can be simulated.

The works mentioned above are based on the hypoplastic model of HP. An approach for applying the original IS concept to different constitutive models, which do not need to include elastic stiffness tensor in their formulation, can be found in Bode et al. (2020). Thereby a so-called *internal elastic* or an *external elastic model* is introduced.

Recently, Alipour and Wu (2023) proposed the incorporation of an additional memory surface within the framework of the classical intergranular strain for the consideration of the stress history of the soil. For this reason, both the strain and the stress history are considered in the constitutive formulation. Based on the hypoplastic formulation of Wu and Bauer (1994) and Wu et al. (1996), overshooting and ratcheting can be reduced (Alipour and Wu, 2023).

5. Generalized intergranular strain concept (GIS)

The IS has been developed as an extension model of the base constitutive HP formulation. The generalized intergranular strain (GIS) approach presented in this work can thereby be easily applied to any kind of constitutive model. It is also based on the tensorial state variable of intergranular strain \mathbf{h} . The well-known evolution Eq. (33) and the corresponding Eqs. (34)–(35) are adopted.

It must be noted that the intergranular strain approaches an asymptotic value due to a sufficiently large monotonic deformation. Asymptotically $\dot{\mathbf{h}} = 0$ is reached at a mobilization of intergranular strain $\rho = 1$. Within the framework of the novel GIS concept, a scalar factor k is defined as:

$$k = [\rho^{\chi_R} m_T + (1 - \rho^{\chi_R}) m_R] + \begin{cases} \rho^{\chi_R} (1 - m_T) \vec{\mathbf{h}} : \dot{\epsilon} & \text{if } \vec{\mathbf{h}} : \dot{\epsilon} > 0 \\ -\rho^{\chi_R} (m_R - m_T) \vec{\mathbf{h}} : \dot{\epsilon} & \text{if } \vec{\mathbf{h}} : \dot{\epsilon} \leq 0. \end{cases} \quad (39)$$

It is worth noting the similarity between the proposed Eq. (39) for the scalar factor k and the interpolation of the tangential stiffness M (Eq. (38)) in the original IS concept. Eq. (39) represents an interpolation for k depending on the current intergranular strain \mathbf{h} , the strain rate $\dot{\epsilon}$ and the mobilization of intergranular strain $\rho = \|\mathbf{h}\|/R$. The material parameter R , m_R , m_T , and χ_R (renamed compared to the original IS concept) can be used to control this interpolation between the maximum value of $k = m_R$ and the minimum value $k = 1$. Four special cases have to be highlighted:

- $k = 1$ and $\rho = 1$ is reached asymptotically due to a sufficient large monotonic strain path.
- $k = m_R$ holds for a 180° loading direction reversal in the case of fully mobilized intergranular strain ($\rho = 1$).
- $k = m_T$ holds for a 90° loading direction reversal in the case of fully mobilized intergranular strain ($\rho = 1$).
- $k = m_R$ holds for $\rho = 0$, independent of the applied strain rate.

In analogy to the visualization of the tangential stiffness M from Niemunis and Herle (1997), Eq. (39) and the discussed special cases are visualized in Fig. 6 in the two-dimensional case. The factor k is thereby a function of the current intergranular strain (h_{11} , h_{22}), its

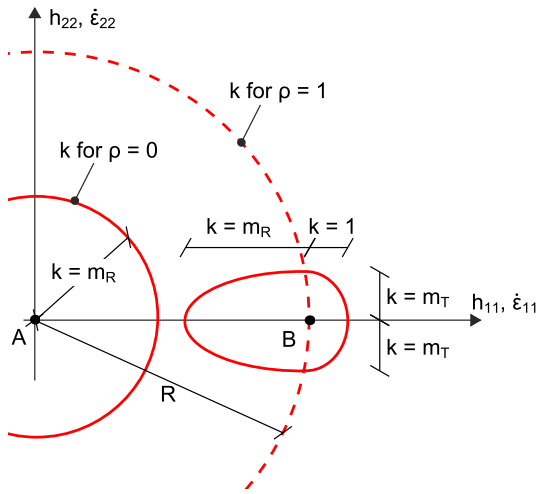


Fig. 6. Scalar factor k with the parameters m_R and m_T for $\rho = 0$ and $\rho = 1$ in the two-dimensional case depending on strain rate $\dot{\epsilon}_{11}$ or $\dot{\epsilon}_{22}$, modified from Niemunis and Herle (1997).

mobilization ρ and the applied strain rate $(\dot{\epsilon}_{11}, \dot{\epsilon}_{22})$. Considering the two aspects of IS mentioned earlier, the factor k can be used further to fulfill the (I) scaling of the stiffness and the (II) reduction of irreversible deformations of the base constitutive model.

In principle, the GIS concept can be applied to all hypoplastic models. For the sake of simplicity, however, only rate-independent hypoplastic formulations for sand are considered as base constitutive model below, which are characterized by the degree of homogeneity of one with respect to the strain rate (Mašín, 2019; Gudehus, 2007). The two purposes of the scalar factor k mentioned above can be taken into account by modifying the Eq. (7) to

$$\dot{\sigma} = k E : \left(\dot{\epsilon} - m C S^{(k\gamma)} \parallel \dot{\epsilon} \parallel + f(\dot{\epsilon}, \alpha) \right), \quad (40)$$

whereby γ can be calculated in accordance to Duque et al. (2020) using the function $\chi(\Omega)$. Thereby, a further historirotropic scalar state variable Ω , which can be physically interpreted as the so-called *cyclic preloading*, is introduced. This state variable considers the amplitude and the number of preloading cycles on the mechanical behavior of soil. Using the material parameter γ_χ , γ can be expressed as

$$\gamma = \gamma_\chi \chi. \quad (41)$$

With the parameters χ_0 and χ_{\max} the function

$$\chi = \chi_0 + \Omega (\chi_{\max} - \chi_0) \quad (42)$$

can be defined. The state variable Ω evolves towards unity ($\Omega \rightarrow 1$) as long as the intergranular strain (IS) is not mobilized $\rho \approx 0$. It vanishes to zero during sufficient long monotonic loading paths or cyclic loading with large strain amplitudes, whereby $\rho \approx 1$ holds. The evolution equation reads

$$\dot{\Omega} = C_\Omega (1 - \rho^\gamma \Omega - \Omega) \parallel \dot{\epsilon} \parallel. \quad (43)$$

If no cyclic preloading is given or known, $\Omega_0 = 0$ can be initialized in practical problems. Details about the historirotropic effects can be found in Duque et al. (2020, 2023c). The exponent γ_Ω has been introduced for generalization. It provides a possibility for controlling the evolution equation of Ω independent of the base constitutive model. It should be noted that $\gamma_\Omega = \gamma$ can be used following Duque et al. (2020) in the case of a coupling with the HP formulation. Four special cases of Eq. (43) can be emphasized:

- $\Omega = 0$ and $\rho = 0$ leads to an increase of Ω with $\dot{\Omega} > 0$.
- $\Omega = 0$ and $\rho = 1$ reduces the evolution of Ω to $\dot{\Omega} = 0$.

- $\Omega = 1$ and $\rho = 0$ reduces the evolution of Ω to $\dot{\Omega} = 0$.
- $\Omega = 1$ and $\rho = 1$ leads to a decrease of Ω with $\dot{\Omega} < 0$.

These limits indicate that $0.0 \leq \Omega \leq 1.0$ applies. The trend of Ω only increases with the number of cycles in the case of an initialization of $\Omega_0 = 0$ and due to a drained cyclic triaxial loading with a prescribed constant deviatoric stress amplitude. Thereby, the so-called *cyclic preloading history* or *historirotropic effects* becomes evident.

It is important to emphasize a further important aspect of the novel GIS formulation. A comparison of Eq. (7) with Eq. (40) reveals that overshooting of a defined state with $S = 1$ of the base constitutive model cannot occur due to the fact that $S = 1$ is not (!) influenced by the GIS modification. In the case of a defined limit state, an overshooting of the overall soil strength is prevented ($S = Y = 1$). In the case of an explicitly defined or even extracted asymptotic state boundary surface (ASBS), overshooting of the ASBS ($S = 1$) is prevented. In other words, even if the state variable of intergranular strain evolves in the strain space, its effect on the mechanical behavior of the soil is limited in the stress space.

This advantage over the original IS model will be demonstrated in Section 6 using numerical examples. It must be noted that the GIS can only improve the intergranular strain concept. The response and the defects of the base constitutive model can of course not be eliminated.

Note furthermore that an original *incrementally non-linear* model remains incrementally non-linear even after coupling with the GIS, whereas using the IS concept, the model becomes *incrementally bi-linear* (Tamagnini and Viggiani, 2002).

In hypoplastic base constitutive models, the GIS approach must modify the irreversible components of the base constitutive model to avoid excessive ratcheting. In the elasto-plastic theory, ratcheting is not a problem due to the elastic un- and reloading. A simple scaling of stiffness in elasto-plastic formulations can however be used to incorporate hysteretic behavior. Elasto-plastic formulations of the general form

$$\dot{\sigma} = E^{\text{el}} : (\dot{\epsilon} - \dot{\epsilon}^{\text{pl}}) \quad (44)$$

can be modified using the GIS by scaling the elastic stiffness:

$$\dot{\sigma} = k E^{\text{el}} : (\dot{\epsilon} - \dot{\epsilon}^{\text{pl}}). \quad (45)$$

Also the elasto-plastic stiffness should be modified using Eq. (45). Nevertheless, this use of the GIS concept in this base model type is not in the focus of the current work. In the following, the GIS concept is demonstrated using the widespread hypoplastic formulation for sand after von Wolffersdorff (1996) (HP+GIS).

6. Hypoplasticity after von Wolffersdorff coupled with generalized intergranular strain (HP+GIS)

The feasibility of the GIS concept and its benefits over the IS concept are demonstrated using the HP as a base constitutive model. The detailed mathematical formulation of HP can be found in Appendix B. As pointed out in Sections 2 and 3, the HP model for sand can be reformulated using the extracted ASBS. Therefore, the HP can be expressed using Eq. (7) with the state mobilization $S = f_d / f_d^{A*}$. The resulting formulation can be coupled further with the GIS concept according to Eq. (40). It is worth mentioning that the HP formulation can also be coupled with the GIS concept using $S = Y$ without considering the extracted ASBS, see Section 2. Such an approach should be used if the ASBS does not exist or cannot be extracted in the base model. However, the formulation including an extracted ASBS is recommended since it prevents the overshooting of the entire ASBS, as explained subsequently in detail.

In addition to the 8 parameters of HP and the 5 parameters of the classical IS concept, 5 parameters for the consideration of the historirotropic effects are needed in the coupled HP+GIS formulation. All the following numerical simulations were carried out using a parameter set for Zbraslav sand, a quartz sand from the vicinity of the Czech

Table 1

Set of constitutive parameters of Zbraslav sand used in this study: (top) parameters for HP, (bottom left) parameters for IS as well as GIS and (bottom right) additional parameters for GIS for the consideration of historiotropic effects, modified from Duque et al. (2023c).

HP									
φ_c	e_{i0}	e_{c0}	e_{d0}	h_s	n	α	β		
[°]	[-]	[-]	[-]	[kPa]	[-]	[-]	[-]	[-]	
34	1.027	0.893	0.520	111 746	0.346	0.15	2.2		
IS/GIS					GIS				
R	m_R	m_T	β_R	χ_R	γ_χ	χ_0	χ_{max}	C_Ω	γ_Ω
[-]	[-]	[-]	[-]	[-]	[-]	[-]	[-]	[-]	[-]
10^{-4}	5	2.5	0.1	4.0	1.7	0.8	1.5	45	1.0

Republic’s capital Prague. Details about the Zbraslav sand can be found in the literature (Duque et al., 2023a,b,c). The original HP+IS model is compared with the new HP+GIS model hereinafter. The parameter set used is given in Table 1. All simulations which follow are performed using the freely available program code *IncrementalDriver* (Niemunis, 2022) and a corresponding implementation of the constitutive formulations using an ABAQUS subroutine *umat.for*. The implementation has been made freely available at the www.soilmodels.com website.

6.1. Prevented overshooting of asymptotic states

As already described and justified theoretically, the GIS concept does not overshoot the ASBS if the base model is formulated using the state mobilization $S = f_d / f_d^{A*}$ since $S = 1$ is not affected. Apart of the more general applicability of the model to different base formulations, this is one of the key advantages of the novel HP+GIS over the old HP+IS. It is demonstrated using element test simulations below.

6.1.1. Triaxial test

First, a drained triaxial compression test on an initially dense sample is considered. The simulations start from an isotropic initial stress state of $p_0 = 100$ kPa and an initial void ratio of $e_0 = 0.595$ ($I_{D0} = 0.8$). The intergranular strain is fully mobilized with $h_{a0} = h_{r0} = -R/\sqrt{3}$ in the initial state and the historiotropic variable is initialized to $\Omega_0 = 0$. Three constitutive formulations are compared: HP, HP+IS, and HP+GIS. Note that for HP+IS the state variable Ω and for HP the state variables Ω and h are not considered.

The drained triaxial compression test considers an unloading of $\Delta\sigma_a = 70$ kPa after $-\epsilon_a = 10\%$ axial strain, followed by a reloading. The resulting deviatoric stress q as a function of the axial strain ϵ_a is illustrated in Fig. 7.

It becomes evident that HP without any small strain overlay model (IS or GIS) exhibits the well-known problem of ratcheting due to the un- and reloading. The stiffness at the reloading stage is thereby comparable (not identical, due to the different void ratios) to the stiffness at virgin loading, which leads to a substantially too soft material response and unrealistically large deformations.

Using HP+IS, the stiffness in the reloading stage is significantly increased compared to the corresponding stiffness at the virgin loading. This prevents ratcheting for certain stress or strain amplitudes. However, the stress–strain curve overshoots the continuation of a previous curve significantly. This results in an overestimation of the strength of the soil, which is called *overshooting* (Duque et al., 2022). It should be mentioned that the simulated unloading corresponds approximately to a strain of $\Delta\epsilon \approx R$ where overshooting is maximally pronounced (Tafili et al., 2024). Note that the overshooting is reduced resp. vanishes for $\Delta\epsilon_a \rightarrow 0$ and for $\Delta\epsilon_a \gg R$.

In HP+GIS, both undesired effects (ratcheting and overshooting) are avoided respectively significantly minimized. The stiffness due to reloading is significantly increased, however, the maximum deviatoric

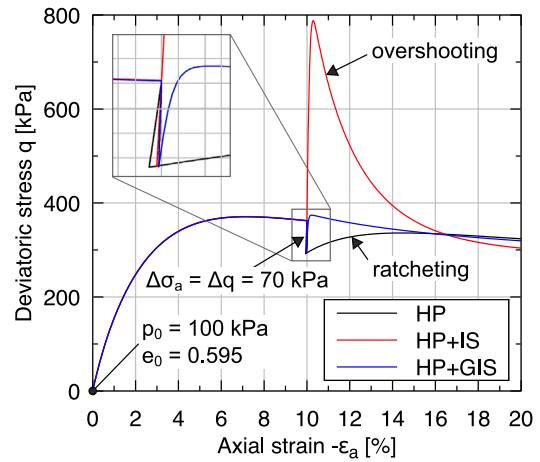


Fig. 7. Drained triaxial tests with an un- and reloading with HP (black), HP+IS (red), and HP+GIS (blue).

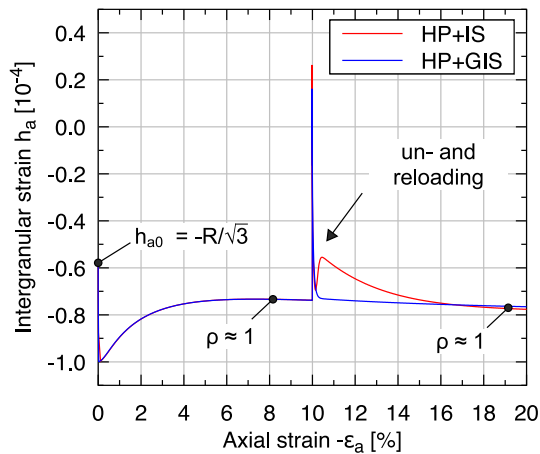


Fig. 8. Intergranular strain component h_a as a function of the axial strain ϵ_a in the drained triaxial test incorporating an unloading of $\Delta\sigma_a = 70$ kPa and subsequent reloading.

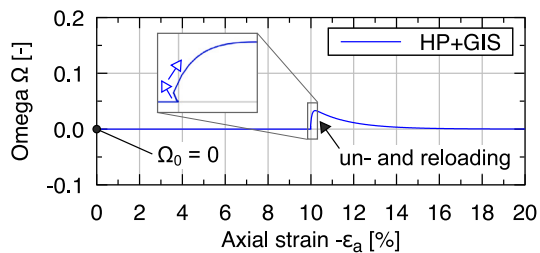


Fig. 9. Historiotropic state variable Ω as a function of the axial strain ϵ_a in the drained triaxial test incorporating an unloading of $\Delta\sigma_a = 70$ kPa and subsequent reloading.

stress exceeds only slightly the expected continued monotonic path from virgin loading. This positive property is attributed to the unaffected state mobilization on the ASBS with $S = 1$, which corresponds in the case of a monotonic triaxial test to the asymptotically reached critical state.

Fig. 8 presents the axial component of intergranular strain h_a as a function of axial strain for the simulations with HP+IS and HP+GIS. Due to the prescribed stress path (even if the simulations must be performed mixed controlled), both models result in slightly different strain paths, which explains the observed differences in the intergranular strain. However, the intergranular strain paths appear very similar.

Before unloading, the intergranular strain is completely mobilized $\rho \approx 1$ due to the monotonic deformation. Significant changes in the intergranular strain occur as a result of changes in the loading direction. Asymptotically, $\rho = 1$ is reached again.

The HP+GIS includes the historiropy variable Ω , whose evolution as a function of axial strain is shown in Fig. 9. It becomes evident that a small build-up of Ω is caused by the change in the direction of loading. However, the subsequent monotonic deformation decreases omega again, leading to an asymptotic value of $\Omega = 0$.

6.1.2. Oedometric test

As described above, the advantages of the formulation of HP using the extracted ASBS consist in the fact that due to $S = 1$ on each asymptotic state, an overshooting of the latter is significantly reduced if the model is coupled with the GIS concept. This is demonstrated in the following using simulations of oedometric compression tests with different initial states. The first one is chosen to be located on the oedometric NCL, which means on the ASBS ($S = 1, f_d = f_d^A = f_d^{A*}$ and a corresponding anisotropic stress state σ^A with $-\sigma_a = 1$ kPa). This state was found iteratively as described in Section 3. In the second initial state, an initial void ratio of $e_0 = 0.873$ ($r_{e0} = 1.0 < r_e^A$) is chosen, which corresponds to $S < 1$. In both initial states, the intergranular strain is initialized to be fully mobilized in axial direction $h_{a0} = -R$, and the historiropic variable is set to $\Omega_0 = 0$.

In addition to the two monotonic paths, simulations with three unloading stages of $\Delta \varepsilon_a = -R$ including the small strain extension and $\Delta \varepsilon_a = -R m_R$ without the small strain extension were conducted. The resulting void ratio e is plotted for all simulations as a function of the axial stress σ_a in Fig. 10a for the simulations using HP+IS and in Fig. 10b using HP+GIS.

First of all, it can be seen that all oedometric compression curves tend asymptotically towards the oedometric NCL. This confirms that the state tends asymptotically to the ASBS. If the IS or GIS concept is not taken into account, the well-known ratcheting can be observed. The latter can be addressed using the IS or the GIS extension. However, it can be seen that simulations with HP+IS leads to a strong overshooting of the corresponding monotonic path. The logarithmic axis should be noted.

For states inside of the ASBS ($S < 1$), an overshooting of the corresponding monotonic path occurs also using the HP+GIS formulation. However, the oedometric NCL (ASBS) is exceeded only slightly and the overshooting of the ASBS ($S = 1$) compared to the HP+IS formulation is significantly reduced. This constitutive property is caused by the reformulated HP model using the extracted ASBS and the coupling with the GIS formulation. It should be noted that the prevented overshooting of an oedometric NCL could not be seen using $S = Y$ instead of $S = f_d/f_d^{A*}$.

However, the small exceed of the monotonic path in the HP+GIS should be discussed briefly. This can be seen in the triaxial test (Fig. 7) as well as in the oedometric test (Fig. 10b). As a result of the unloading, the current state of the soil changes. The resulting value of f_d^{A*} upon reloading therefore does not correspond to the one of the virgin loading. Strictly speaking, the asymptotic state assumed in the base model at the beginning of the reloading and does not correspond to the one at the beginning of the unloading. These changes in the state also occur for the simulations without the GIS concept using only the HP. However, due to the much smaller stiffness without the GIS extension, the path does not exceed the monotonic one. Combined with the increased stiffness due to the GIS concept, slight overshooting may result.

6.2. Accumulation due to undrained cyclic loading

Accumulative effects due to cyclic deformation in the soil pose a major challenge for constitutive modeling. In the original IS concept, these accumulation effects occur as by-products of the calculation

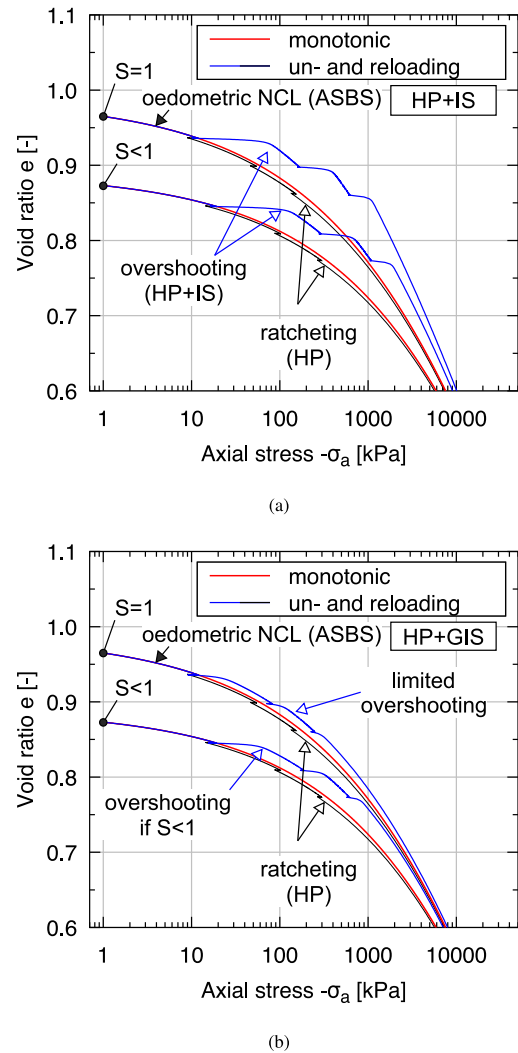
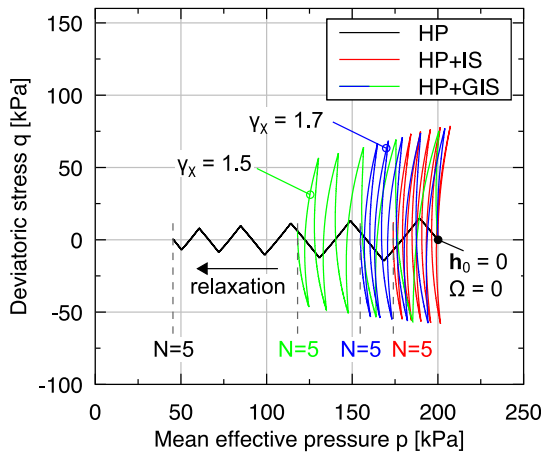


Fig. 10. Oedometric compression tests with monotonic deformation (red) and three small un- and reloading stages simulated using the HP model with (blue) and without (black) small strain overlay models: (a) HP+IS and (b) HP+GIS.

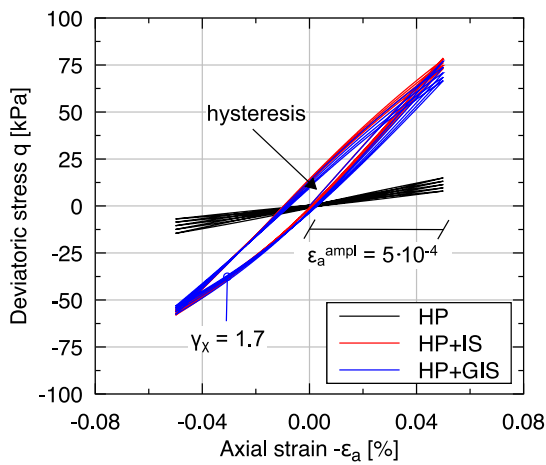
and could not be directly influenced. It must also be mentioned that (artificial) accumulation can occur as a result of a hypoelastic behavior of the base constitutive model (Poblete et al., 2016; Mugele et al., 2024a). To avoid this, a hyperelastic stiffness should be introduced in the base constitutive model, as for example in Grandas-Tavera et al. (2020) and Mugele et al. (2024b). It needs to be emphasized that the HP includes a hypoelastic linear part and therefore artificial accumulations can occur.

Assuming that the artificial accumulation effects can be neglected, the accumulation rate due to cyclic deformation can be mainly controlled in HP+GIS by adjusting the parameter γ_χ . To illustrate this, a cyclic undrained triaxial test with a prescribed strain amplitude of $\varepsilon_a^{ampl} = -2 \varepsilon_r^{ampl} = 5 \cdot 10^{-4}$ is considered. The simulations start at an isotropic stress state of $p_0 = 200$ kPa, a void ratio of $e_0 = 0.6915$ ($I_{D0} = 0.5$), an intergranular strain of $h_0 = \mathbf{0}$, and a historiropic variable of $\Omega_0 = 0$. Five subsequent cycles are simulated. Fig. 11a shows the resulting stress path in the pq diagram for simulations using HP, HP+IS, and HP+GIS. Two values of γ_χ are used in the latter case ($\gamma_\chi = 1.7$ and $\gamma_\chi = 1.5$). The resulting stress-strain curves are shown in Fig. 11b.

It can be seen that the base constitutive model HP alone results in excessive stress relaxation. In addition, there is almost no hysteretic behavior. On the other hand, HP+IS, leads to a realistic accumulation



(a)



(b)

Fig. 11. Undrained cyclic triaxial tests with predefined strain amplitude $\epsilon_a^{ampl} = 5 \cdot 10^{-4}$ for HP (black), HP+IS (red) and HP+GIS (blue): (a) stress path in the pq diagram and (b) deviation stress q as a function of axial strain ϵ_a .

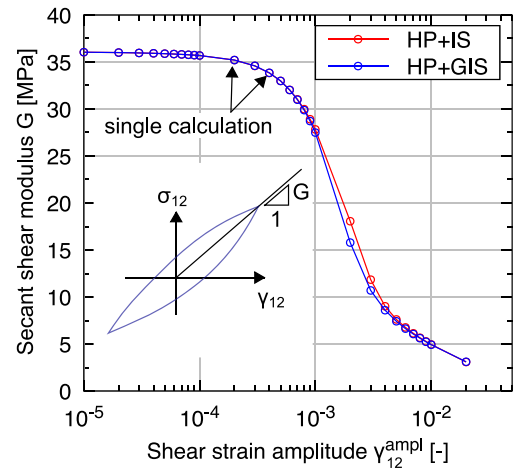
and hysteric behavior. However, the accumulation rate in the HP+IS cannot be controlled. The hysteric behavior is achieved through a significant increase in stiffness after a load direction reversal, see Fig. 11b.

The use of HP+GIS also results in a pronounced hysteric behavior. In addition, the accumulation effects can be influenced by adjusting the material parameter γ_x . Larger values of γ_x lead to lower accumulation effects. The slightly changing hysteric curves of the simulations using HP+GIS are due to different mean effective pressure and due to historiotropic effects which are discussed in detail in Section 6.4.

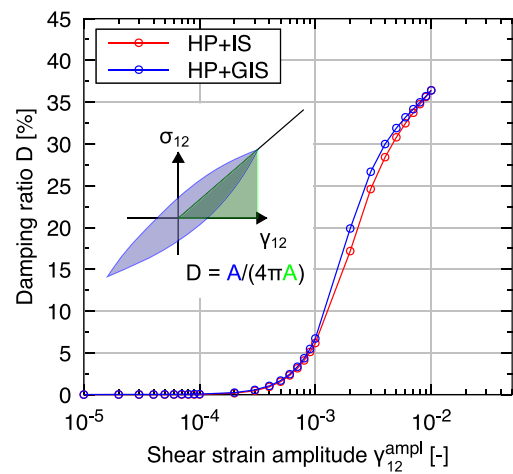
6.3. Stiffness degradation and damping curves

The secant shear stiffness modulus G of soil is strongly dependent on the corresponding shear strain amplitude γ^{ampl} . The stiffness is significantly higher at small shear strain amplitudes than at larger ones. As the shear strain amplitude increases, the damping of the material also increases. Damping can be neglected for small shear strains with high stiffness. These effects can have significant relevance in solving geotechnical problems (Simpson, 1992; Benz et al., 2009b; Cudny and Truty, 2020) and should therefore be considered adequately.

Essentially, these small-strain effects can be modeled using both HP+IS and HP+GIS, as these overlay models are designed to address



(a)

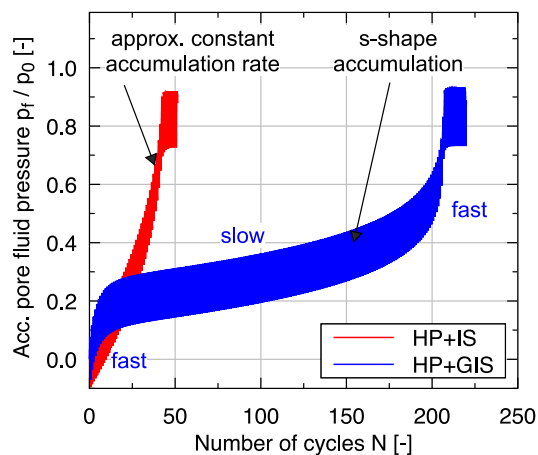


(b)

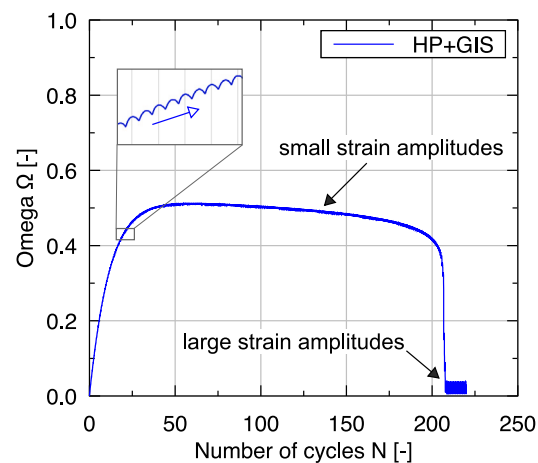
Fig. 12. Cyclic simple shear tests with varying shear strain amplitude using the HP+IS and HP+GIS: (a) secant shear stiffness modulus G and (b) damping ratio D as a function of the shear strain amplitude γ_{12}^{ampl} for HP+IS (red) and HP+GIS (blue).

them. However, the question arises whether the new GIS concept is comparable to the original IS concept. To calculate the secant stiffness degradation as a function of the applied shear strain amplitude and the corresponding damping curve, cyclic simple shear tests with $\dot{\sigma}_{11} = 0 = \dot{\epsilon}_{22} = \dot{\epsilon}_{33} = \dot{\epsilon}_{13} = \dot{\epsilon}_{23}$ and a variation of the shear strain amplitude $\epsilon_{12}^{ampl} = 0.5\gamma_{12}^{ampl}$ are considered. In all simulations, an isotropic initial stress state of $p_0 = 100$ kPa, a void ratio of $e_0 = 0.6915$ ($I_{D0} = 0.5$), an intergranular strain $h_0 = \mathbf{0}$, and the historiotropic variable $\Omega_0 = 0$ is initialized.

The secant shear stiffness G and the damping D can be calculated in the post-processing using the resulting hysteric $\sigma_{12} - \gamma_{12}$ curves. The 3rd cycle of the cyclic simple shear tests is therefore used in this study. Fig. 12a visualizes the resulting degradation curve of the secant shear stiffness and Fig. 12b the corresponding damping curve for both the HP+IS and HP+GIS models. Note that in these figures the mathematical derivation of stiffness modulus G and damping ratio D is shown graphically. The GIS concept leads to very similar curves compared to the IS concept, which corresponds to the generally expected soil behavior. Based on a high stiffness and negligible damping at small strains, the stiffness reduces, and the damping increases with increasing shear strain amplitude.



(a)



(b)

Fig. 13. Undrained cyclic triaxial tests with predefined stress amplitude $q^{\text{amp}} = 50$ kPa for HP+IS (red) and HP+GIS (blue): (a) accumulation of normalized pore fluid pressure p_f/p_0 and (b) evolution of the state variable Ω with the number of cycles N .

6.4. Historiotropic effects

Accumulative effects in soil due to cyclic loading are highly non-linear with respect to the number of cycles N . These historiotropic effects can be seen for example in the well-known s-shaped pore fluid pressure accumulation curves in undrained triaxial tests with stress cycles (Duque et al., 2023b,a). Historiotropic effects are considered in the GIS concept following Duque et al. (2020) by the additional scalar state variable Ω , see Eqs. (41)–(43).

To demonstrate the effect of Ω , a cyclic and undrained triaxial test with a stress amplitude $q^{\text{amp}} = 50$ kPa is analyzed. An isotropic stress state $p_0 = 200$ kPa, a void ratio of $e_0 = 0.6915$ ($I_{D0} = 0.5$), an intergranular strain $h_0 = \mathbf{0}$, and $\Omega_0 = 0$ is initialized. For such tests, so-called s-shaped curves representing the accumulation of the pore fluid pressure p_f as a function of the number of cycles N are expected (Wichtmann, 2016; Wichtmann and Triantafyllidis, 2016; Duque et al., 2023a,b). The build-up of pore fluid pressure is fast for the first cycles, followed by a slower and finally a faster accumulation.

The simulated curves of the pore fluid pressure accumulation resulting from HP+IS and HP+GIS are shown in Fig. 13a. It can be seen that the accumulation rate is almost constant in simulations with the HP+IS. This leads to an accumulation of pore fluid pressure that is

approximately proportional to the number of cycles, which is not consistent with experimental observations (Wichtmann, 2016; Wichtmann and Triantafyllidis, 2016; Duque et al., 2023a,b).

In contrast, the calculation using HP+GIS including the state variable Ω shows the expected experimentally observed s-shaped curve of the pore fluid pressure accumulation. The variation of the accumulation rate is attributed to the state variable Ω . Its evolution is shown in Fig. 13b. The smaller Ω , the faster the accumulation. Ω is small due to the corresponding initialization at the beginning and due to the large strain amplitudes at the end of the simulation. In between, there is a build-up of Ω due to small shear strain amplitudes (Duque et al., 2020).

7. Conclusion

In this work, the generalized intergranular strain (GIS) approach, based on the intergranular strain concept (IS) after Niemunis and Herle (1997) resp. the intergranular strain improvement (ISI) formulation after Duque et al. (2020), is introduced and its feasibility is demonstrated using simulations with the base constitutive model of hypoplasticity after von Wolffersdorff (1996) (HP). The latter is expressed using an extracted asymptotic state boundary surface (ASBS). Using this formulation, the ASBS can also be visualized for sand. The GIS approach presented here shows three major advantages over the base version of IS:

1. The approach can be adopted to other hypoplastic and also non-hypoplastic models.
2. The approach prevents the overshooting effect.
3. Accumulative effects can be realistically modeled while taking historiotropic effects with an additional scalar state variable Ω into account. The latter advantage is adopted from the ISI formulation.

Finally, it should be noted that the shortcomings of the base HP model are beyond the scope of the current paper. Some of them have recently been discussed in the context of neohypoplasticity (NHP) (Niemunis et al., 2016; Niemunis and Grandas-Tavera, 2019; Mugele et al., 2024b).

CRedit authorship contribution statement

L. Mugele: Writing – original draft, Visualization, Software, Methodology, Investigation, Funding acquisition, Conceptualization. **H.H. Stutz:** Writing – review & editing, Supervision, Resources, Project administration, Methodology, Funding acquisition, Conceptualization. **D. Mašín:** Writing – review & editing, Validation, Supervision, Resources, Project administration, Methodology, Funding acquisition, Conceptualization.

Declaration of competing interest

The authors declare that they have no known competing financial interests or personal relationships that could have appeared to influence the work reported in this paper.

Data availability

Data will be made available on reasonable request. An implementation of the HP+GIS model in terms of a umat.for subroutine has been made freely available on the www.soilmodels.com website.

Acknowledgments

The first author acknowledges the research gravel grant from Karlsruhe House of Young Scientists (KHYS) for the financial support for the stay at Charles University Prague. The first author would also like to express gratitude to the entire team at Charles University Prague for their gracious hospitality. The third author is grateful for the financial support given by the grant No. 21-35764J of the Czech Science Foundation.

Appendix A. Notation and abbreviations

The conventional mechanical sign convention is used throughout this paper. Extension strains and tensile stress are therefore positive. Second-order tensors are written in bold letters (e.g. σ or N), with $\|\cdot\|$ denoting the Euclidean norm and $\text{tr}(\cdot)$ representing the sum of diagonal components of the corresponding tensor \cdot . Normalized tensors are denoted as $\hat{\cdot} = \cdot / \|\cdot\|$. The deviatoric part of a second-order tensor \cdot is denoted with $\hat{\cdot}^*$. Fourth-order tensors are symbolized using capital sans-serif letters (e.g. M). The symbol \cdot denotes multiplication with one dummy index (single contraction), for instance, the scalar product of two first-order tensors can be written as $a \cdot b$. The multiplication with two dummy indices (double contraction) is written using a colon, for example, $A : B$. Dyadic multiplication is written as ab . The unit tensor of second-order (δ) and fourth-order tensor (I) are defined. Stresses are effective in the sense of Terzaghi and the Roscoe invariants $p = -\text{tr}(\sigma)/3$ and $q = \sigma_r - \sigma_a = \sigma_2 - \sigma_1$ are used for triaxial stress states. The following abbreviations are considered:

ASBS	Asymptotic state boundary surface
NCL	Normal compression line
HP	Hypoplasticity after von Wolffersdorff (1996) (HP)
NHP	Neohypoplasticity (Niemunis et al., 2016; Niemunis and Grandas-Tavera, 2019; Mugele et al., 2024b)
IS	Intergranular strain after Niemunis and Herle (1997)
ISA	Intergranular strain anisotropy (Fuentes and Triantafyllidis, 2015)
ISI	Intergranular strain improvement (Duque et al., 2020)
GIS	Proposed generalized intergranular strain concept

Appendix B. HP formulation after von Wolffersdorff (1996)

This appendix summarizes the mathematical formulation of the hypoplastic model after von Wolffersdorff (1996) (HP). The model assumes the relation between the stress rate and the strain rate

$$\dot{\sigma} = f_s L : \dot{\epsilon} + f_d N \|\dot{\epsilon}\| \dot{\epsilon} \quad (\text{B.1})$$

with

$$L = \frac{1}{\hat{\sigma} : \hat{\sigma}} (F^2 I + a^2 \hat{\sigma} \hat{\sigma}) \quad (\text{B.2})$$

and

$$N = \frac{Fa}{\hat{\sigma} : \hat{\sigma}} (\hat{\sigma} + \hat{\sigma}^*), \quad (\text{B.3})$$

where $I_{ijkl} = 0.5(\delta_{ik}\delta_{jl} + \delta_{il}\delta_{jk})$ is a fourth-order unity tensor and δ is a second-order unity tensor with

$$\hat{\sigma} = \frac{\sigma}{\text{tr}(\sigma)} \quad \text{and} \quad \hat{\sigma}^* = \hat{\sigma} - \frac{1}{3}\delta \quad (\text{B.4})$$

with

$$a = \sqrt{\frac{3}{8}} \frac{(3 - \sin \varphi_c)}{\sin \varphi_c} \quad (\text{B.5})$$

and

$$F = \sqrt{\frac{1}{8} \tan^2 \psi + \frac{2 - \tan^2 \psi}{2 + \sqrt{2} \tan \psi \cos(3\theta)}} - \frac{1}{2\sqrt{2}} \tan \psi \quad (\text{B.6})$$

with

$$\tan \psi = \sqrt{3} \|\hat{\sigma}^*\| \quad (\text{B.7})$$

and

$$\cos(3\theta) = -\sqrt{6} \frac{\text{tr}(\hat{\sigma}^* \cdot \hat{\sigma}^* \cdot \hat{\sigma}^*)}{[\hat{\sigma}^* : \hat{\sigma}^*]^{3/2}}. \quad (\text{B.8})$$

The scalar factors f_s and f_d take into account the influence of mean effective pressure and density:

$$f_s = \frac{h_s}{n} \left(\frac{e_i}{e}\right)^\beta \frac{1 + e_i}{e_i} \left(\frac{-\text{tr} \sigma}{h_s}\right)^{1-n} \left[3 + a^2 - a\sqrt{3} \left(\frac{e_{i0} - e_{d0}}{e_{c0} - e_{d0}}\right)^\alpha\right]^{-1}, \quad (\text{B.9})$$

$$f_d = \left(\frac{e - e_d}{e_c - e_d}\right)^\alpha. \quad (\text{B.10})$$

The characteristic void ratios (e_i , e_c and e_d) decrease with the mean pressure according to the relation

$$\frac{e_i}{e_{i0}} = \frac{e_d}{e_{d0}} = \frac{e_c}{e_{c0}} = \exp \left[- \left(\frac{3p}{h_s} \right)^n \right]. \quad (\text{B.11})$$

The model requires 8 parameters: φ_c , h_s , n , e_{d0} , e_{c0} , e_{i0} , α and β .

References

- Alipour, M.-J., Wu, W., 2023. Hypoplastic model with an inner memory surface for sand under cyclic loading. *Comput. Geotech.* 162, 105666.
- Bauer, E., 1996. Calibration of a comprehensive hypoplastic model for granular materials. *Soils Found.* 36 (1), 13–26.
- Benz, T., Schwab, R., Vermeer, P., 2009a. Small-strain stiffness in geotechnical analyses. *Bautechnik* 86 (S1), 16–27.
- Benz, T., Vermeer, P.A., Schwab, R., 2009b. A small-strain overlay model. *Int. J. Numer. Anal. Methods Geomech.* 33 (1), 25–44.
- Bode, M., Fellin, W., Mašin, D., Medicus, G., Ostermann, A., 2020. An intergranular strain concept for material models formulated as rate equations. *Int. J. Numer. Anal. Methods Geomech.* 44 (7), 1003–1018.
- Bode, M., Fellin, W., Medicus, G., 2021. Reloading in barodesy employing the asymptotic state boundary surface. *Int. J. Numer. Anal. Methods Geomech.* 45 (14), 2113–2129.
- Chrisopoulos, S., Vogelsang, J., 2019. A finite element benchmark study based on experimental modeling of vibratory pile driving in saturated sand. *Soil Dyn. Earthq. Eng.* 122, 248–260.
- Cudny, M., Truty, A., 2020. Refinement of the hardening soil model within the small strain range. *Acta Geotech.* 15 (8), 2031–2051.
- Duque, J., Mašin, D., Fuentes, W., 2020. Improvement to the intergranular strain model for larger numbers of repetitive cycles. *Acta Geotech.* 15 (12), 3593–3604.
- Duque, J., Roháč, J., Mašin, D., 2023a. On the influence of drained cyclic preloadings on the cyclic behaviour of Zbraslav sand. *Soil Dyn. Earthq. Eng.* 165, 107666.
- Duque, J., Roháč, J., Mašin, D., Najser, J., Opršal, J., 2023b. The influence of cyclic preloadings on cyclic response of Zbraslav sand. *Soil Dyn. Earthq. Eng.* 166, 107720.
- Duque, J., Tafili, M., Mašin, D., 2023c. On the influence of cyclic preloadings on the liquefaction resistance of sands: A numerical study. *Soil Dyn. Earthq. Eng.* 172, 108025.
- Duque, J., Yang, M., Fuentes, W., Mašin, D., Taiebat, M., 2022. Characteristic limitations of advanced plasticity and hypoplasticity models for cyclic loading of sands. *Acta Geotech.* 17 (6), 2235–2257.
- Fuentes, W., Triantafyllidis, T., 2015. ISA model: A constitutive model for soils with yield surface in the intergranular strain space. *Int. J. Numer. Anal. Methods Geomech.* 39 (11), 1235–1254.
- Grandas-Tavera, C.E., Triantafyllidis, T., Knittel, L., 2020. A constitutive model with a historyotropic yield surface for sands. In: *Recent Developments of Soil Mechanics and Geotechnics in Theory and Practice*. Springer, Cham, pp. 13–43.
- Gudehus, G., 1996. A comprehensive constitutive equation for granular materials. *Soils Found.* 36 (1), 1–12.
- Gudehus, G., 2007. *Physical Soil Mechanics*. Springer.
- Gudehus, G., Mašin, D., 2009. Graphical representation of constitutive equations. *Géotechnique* 59 (2), 147–151.
- Jerman, J., Mašin, D., 2020. Hypoplastic and viscohypoplastic models for soft clays with strength anisotropy. *Int. J. Numer. Anal. Methods Geomech.* 44 (10), 1396–1416.
- Kolymbas, D., 1988. *Eine konstitutive Theorie für Böden und andere körnige Stoffe* (Habilitation). Institute for Soil Mechanics and Rock Mechanics, Karlsruhe Institute of Technology, No. 109.
- Kolymbas, D., 1991a. Computer-aided design of constitutive laws. *Int. J. Numer. Anal. Methods Geomech.* 15 (8), 593–604.
- Kolymbas, D., 1991b. An outline of hypoplasticity. *Arch. Appl. Mech.* 61 (3), 143–151.
- Liao, D., Yang, Z.X., 2021. Hypoplastic modeling of anisotropic sand behavior accounting for fabric evolution under monotonic and cyclic loading. *Acta Geotech.* 16 (7), 2003–2029.
- Liao, D., Yang, Z., Wang, S., Wu, W., 2022. Hypoplastic model with fabric change effect and semifluidized state for post-liquefaction cyclic behavior of sand. *Int. J. Numer. Anal. Methods Geomech.* 46 (17), 3154–3177.
- Machaček, J., Staubach, P., Tafili, M., Zacher, H., Wichtmann, T., 2021. Investigation of three sophisticated constitutive soil models: From numerical formulations to element tests and the analysis of vibratory pile driving tests. *Comput. Geotech.* 138, 104276.
- Matsuoka, H., Nakai, T., 1977. Stress-strain relationship of soil based on the SMP, constitutive equations of soils. In: Murayama, S., Schofield, A.N. (Eds.), *Speciality Session 9*.
- Mašin, D., 2005. A hypoplastic constitutive model for clays. *Int. J. Numer. Anal. Methods Geomech.* 29 (4), 311–336.

- Mašín, D., 2009. Comparison of predictive capabilities of selected elasto-plastic and hypoplastic models for structured clays. *Soils Found.* 49 (3), 381–390.
- Mašín, D., 2012. Hypoplastic cam-clay model. *Géotechnique* 62 (6), 549–553.
- Mašín, D., 2013. Clay hypoplasticity with explicitly defined asymptotic states. *Acta Geotech.* 8 (5), 481–496.
- Mašín, D., 2014. Clay hypoplasticity model including stiffness anisotropy. *Géotechnique* 64 (3), 232–238.
- Mašín, D., 2019. *Modelling of Soil Behaviour with Hypoplasticity*. Springer International Publishing, Cham.
- Mašín, D., Herle, I., 2005. State boundary surface of a hypoplastic model for clays. *Comput. Geotech.* 32 (6), 400–410.
- Mašín, D., Herle, I., 2006. State boundary surface in hypoplasticity. In: Wu, W., Yu, H.-S. (Eds.), *Modern Trends in Geomechanics*. In: Springer Proceedings in Physics, Springer, Berlin, pp. 117–128.
- Mašín, D., Rott, J., 2014. Small strain stiffness anisotropy of natural sedimentary clays: review and a model. *Acta Geotech.* 9 (2), 299–312.
- Mugele, L., Mašín, D., Stutz, H.H., 2024a. Neohypoplasticity for sand coupled with the generalized intergranular strain concept. (in preparation).
- Mugele, L., Niemunis, A., Stutz, H.H., 2024b. Neohypoplasticity revisited. *Int. J. Numer. Anal. Methods Geomech.* 48 (1), 311–331.
- Niemunis, A., 2003. *Extended Hypoplastic Models for Soils (Habilitation)*. Schriftenreihe des Institutes für Grundbau und Bodenmechanik der Ruhr-Universität Bochum, No. 34.
- Niemunis, A., 2022. *IncrementalDriver: Programmer's Manual*. <https://soilmodels.com/idriver/>.
- Niemunis, A., Grandas-Tavera, C.E., 2019. Essential concepts of neohypoplasticity. In: Wu, W. (Ed.), *Desiderata Geotechnica*. In: Springer eBooks Engineering, Springer, Cham, pp. 132–142.
- Niemunis, A., Grandas-Tavera, C.E., Prada-Sarmiento, L.F., 2009. Anisotropic visco-hypoplasticity. *Acta Geotech.* 4 (4), 293–314.
- Niemunis, A., Grandas-Taverna, C.E., Wichtmann, T., 2016. Peak stress obliquity in drained and undrained sands. Simulations with neohypoplasticity. In: *Holistic Simulation of Geotechnical Installation Processes*. Springer, Cham, pp. 85–114.
- Niemunis, A., Herle, I., 1997. Hypoplastic model for cohesionless soils with elastic strain range. *Mech. Cohesive-Frict. Mater.* 2 (4), 279–299.
- Norlyk, P., Sørensen, K., Andersen, L.V., Sørensen, K.K., Stutz, H.H., 2020. Holistic simulation of a subsurface inflatable geotechnical energy storage system using fluid cavity elements. *Comput. Geotech.* 127, 103722.
- Osinov, V.A., 2005. Large-strain dynamic cavity expansion in a granular material. *J. Engrg. Math.* 52 (1–3), 185–198.
- Osinov, V.A., 2017. Some aspects of the boundary value problems for the cyclic deformation of soil. In: *Holistic Simulation of Geotechnical Installation Processes*, vol. 82, Springer, Cham, pp. 150–167.
- Poblete, M., Fuentes, W., Triantafyllidis, T., 2016. On the simulation of multidimensional cyclic loading with intergranular strain. *Acta Geotech.* 11 (6), 1263–1285.
- Simpson, B., 1992. *Retaining structures: displacement and design*. *Géotechnique* 42 (4), 541–576.
- Staubach, P., Macháček, J., Wichtmann, T., 2021. Large-deformation analysis of pile installation with subsequent lateral loading: Sanisand vs. Hypoplasticity. *Soil Dyn. Earthq. Eng.* 151, 106964.
- Stutz, H.H., Norlyk, P., Sørensen, K., Andersen, L.V., Sørensen, K.K., Clausen, J., 2020. Finite element modelling of an energy-geomembrane underground pumped hydro-electric energy storage system. *E3S Web of Conferences*, E3S Web of Conferences, vol. 205.07001,
- Tafili, M., Duque, J., Mašín, D., Wichtmann, T., 2024. Repercussion of overshooting effects on elemental and finite-element simulations. *Int. J. Geomech.* 24 (3).
- Tamagnini, C., Viggiani, G., 2002. Constitutive modelling for rate-independent soils: A review. *Revue Française Génie Civ.* 6 (6), 933–974.
- von Wolffersdorff, P.-A., 1996. A hypoplastic relation for granular materials with a predefined limit state surface. *Mech. Cohesive-Frict. Mater.* 1 (3), 251–271.
- Wegener, D., Herle, I., 2014. Prediction of permanent soil deformations due to cyclic shearing with a hypoplastic constitutive model. *geotechnik* 37 (2), 113–122.
- Wichtmann, T., 2016. *Soil Behaviour Under Cyclic Loading - Experimental Observations, Constitutive Description and Applications (Habilitation)*. Institute for Soil Mechanics and Rock Mechanics, Karlsruhe Institute of Technology, No. 181.
- Wichtmann, T., Triantafyllidis, T., 2016. An experimental database for the development, calibration and verification of constitutive models for sand with focus to cyclic loading: part I—tests with monotonic loading and stress cycles. *Acta Geotech.* 11 (4), 739–761.
- Wotzlaw, M., Aubram, D., Rackwitz, F., 2023. Numerical analysis of deep vibrocompaction at small and full scale. *Comput. Geotech.* 157, 105321.
- Wu, W., 1992. *Hypoplastizität als mathematisches Modell zum mechanischen Verhalten granularer Stoffe (Dissertation)*. Institute for Soil Mechanics and Rock Mechanics, Karlsruhe Institute of Technology, No. 129.
- Wu, W., Bauer, E., 1994. A simple hypoplastic constitutive model for sand. *Int. J. Numer. Anal. Methods Geomech.* 18 (12), 833–862.
- Wu, W., Bauer, E., Kolymbas, D., 1996. Hypoplastic constitutive model with critical state for granular materials. *Mech. Mater.* 23 (1), 45–69.